THE SEISMOLOGICAL SOCIETY OF AMERICA
400 Evelyn Ave., Suite 201
Albany, CA 94706-1375
(510) 525-5474; FAX (510) 525-7204
www.seismosoc.org

Bulletin of the Seismological Society of America, Vol. 106, No. 6, pp. –, December 2016, doi: 10.1785/0120150344

Earthquake Source Properties from Pseudotachylite

by N. M. Beeler, Giulio Di Toro,* and Stefan Nielsen

Abstract Earthquake-radiated motions contain information that can be interpreted as source displacement and therefore related to stress drop. Except in a few notable cases, these displacements cannot be easily related to the absolute stress level or the fault strength, or attributed to a particular physical mechanism. In contrast, paleoearthquakes recorded by exhumed pseudotachylite have a known dynamic mechanism whose properties constrain the coseismic fault strength. Pseudotachylite can be used to directly address a discrepancy between seismologically measured stress drops, which are typically a few MPa, and much larger dynamic stress drops expected from thermal weakening during slip at seismic speeds in crystalline rock (Mckenzie and Brune, 1972; Sibson, 1973; Lachenbruch, 1980; Mase and Smith, 1987; Rice, 2006), and as have been observed in laboratory experiments at high slip rates (Di Toro, Hirose, Nielsen, Pennacchioni, *et al.*, 2006). This places pseudotachylite-derived estimates of fault strength and inferred crustal stress within the context and bounds of naturally observed earthquake source parameters: apparent stress, stress drop, and overshoot, including consideration of fault-surface roughness, off-fault damage, fracture energy, and the strength excess. The analysis, which assumes stress drop is related to corner frequency as in the Madariaga (1976) source model, is restricted to earthquakes of the Gole Larghe fault zone in the Italian Alps, where the dynamic shear strength is well constrained by field and laboratory measurements. We find that radiated energy is similar to or exceeds the shear-generated heat and that the maximum strength excess is ∼16 MPa. These events have inferred earthquake source parameters that are rare, for instance, a low percentage of the global earthquake population has stress drops as large, unless fracture energy is routinely greater than in existing models, pseudotachylite is not representative of the shear strength during the earthquake that generated it, or the strength excess is larger than we have allowed.

Introduction

Within the earthquake source region, a large number of inelastic processes are thought to operate: frictional sliding, rock fracture, dilatancy, melting, devolatilization, thermal expansion of pore fluid, hydrofracture, and creation of new fracture surface energy are among many known and proposed processes (Andrews, 1976; Scholz, 2002; Rice, 2006). The processes that actually occur depend on mineralogy, ambient temperature and stress conditions, total slip, the degree of shear localization, the amount of shear dilatancy, and fault-zone hydraulic properties. Outside the source, the surrounding rock is assumed predominantly elastic, and the motions radiated from the source as elastodynamic waves can be related to the spatial time history of displacement within the source. Accounting for attenuation, scattering, and other path effects, information propagating from the source is interpretable at the surface in terms of, for example, source stress drop, moment, radiated energy, and displacement or velocity spectrum, but only on rare occasions to the absolute level of stress (e.g., Spudich, 1992). As for earthquakes that have source mechanisms that are predominately double couple, to date there is little observational or theoretical research that ties surface-recorded motions to a particular physical mechanism within the source. Hence, with the exception of a very few notable claims (e.g., Kanamori *et al.*, 1998), which source processes actually occur for any particular earthquake is anyone's guess.

Field Observations and Melt Shear Strength

A well-understood exception is the ancient earthquakes recorded in exhumed pseudotachylites (Sibson, 1975). Pseudotachylite is thought by most to be the definitive record of an earthquake where dynamic strength was controlled by shear melting (Jeffreys, 1942; McKenzie and Brune, 1972; Sibson,

*Also at Dipartimento di Geoscienze, Università degli Studi di Padova, Padova, Italy.

1975), though there are alternative interpretations (e.g., Pec *et al.*, 2012, and references therein). In the present study, we assume that natural pseudotachylites are generated by coseismic shear heating and take advantage of field and laboratory constraints on the coseismic properties of the shear zone. Melt layers are viscous and therefore have strengths that are quite strongly slip-rate and thickness dependent. In addition, the viscosity can depend on the characteristics of the flow regime and melt composition (Spray, 1993; Lavallee *et al.*, 2015). The field measurements avoid these complexities and produce empirical constraints on the dynamic shear strength during the event (Sibson, 1975). Specifically, field-measured values of the thickness of a pseudotachylite layer w are used with the protolith heat capacity to estimate the heat necessary to melt a particular volume of rock of a particular composition. Sibson assumed all the shear-generated heat remains in the slipping zone and causes constituent minerals to melt immediately upon reaching the melting temperature T_m. Somewhat more recently Wenk *et al.* (2000) and Di Toro *et al.* (2005) repeated the same type of analysis while also allowing for some of the shear heat to be absorbed in the slipping zone as latent heat of fusion. Accordingly, the heat necessary to convert a thickness of rock to melt entirely is

$$Q = A\rho w[(T_m - T_0)c_p + H], \tag{1a}$$

in which c_p is the heat capacity (energy/mass K), H is the heat of fusion (in energy/mass), A is the fault area, ρ is the density (mass/volume), and T_0 is the initial slipping-zone temperature. The two terms on the right side of equation (1a) are from left to right, the change in thermal energy within the slipping zone and the energy necessary to drive the endothermic melting reaction, the latent heat stored within the melt. This assumes that significant heat does not diffuse away from the fault coseismically, which is reasonable given the low thermal diffusivity of rocks ($\kappa \approx 10^{-6}$ m^2 s^{-1}) and the few-second duration Δt of earthquake slip (Lachenbruch, 1980), which results in a heat penetration distance $z \approx \sqrt{\kappa \Delta t} < 2$–$3$ mm. An additional requirement of equation (1a) is that the slipping-zone temperature does not exceed the melting temperature (no superheating), which is expected if the phase change buffers the temperature increase. The displacement-averaged shear strength is

$$\hat{\tau}_m = \frac{Q}{A\Delta\delta}, \tag{1b}$$

in which $\Delta\delta$ is the fault slip as measured in the field using offset markers across the fault (Sibson, 1975). Combining equations (1a) and (1b), the displacement-averaged shear strength during seismic slip that produces a shear melt is

$$\hat{\tau}_m = \frac{\rho w}{\Delta\delta}[(T_m - T_0)c_p + H]. \tag{1c}$$

The heat of fusion is on the order of 10^5 J/kg, whereas the heat capacity is of order 10^3 J/kgK for granitic compositions. As long as the temperature difference $T_m - T_0$ is

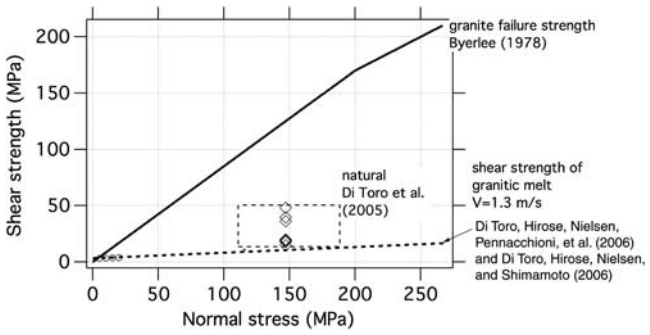

Figure 1. Natural and laboratory observed shear strength of granitic melt. The approximate static strength of pre-existing faults in granitic rocks (solid line; Byerlee, 1978) is shown for reference. The dashed line is the regression of experimental data from Di Toro, Hirose, Nielsen, and Shimamoto (2006), extrapolated to higher normal stress. The field-inferred shear strengths of Di Toro *et al.* (2005) and Di Toro, Hirose, Nielsen, Pennacchioni, *et al.* (2006), that are calculated from measured thickness–displacement ratios using equation (1c), are plotted as the open symbols at the inferred mean normal stress. The box shows the range of possible field-inferred shear and normal stresses.

1000 K or more, the change in thermal energy greatly exceeds the heat of fusion and dominates the sum (1c). This is the case for both the natural (Di Toro *et al.*, 2005) and laboratory (Di Toro, Hirose, Nielsen, Pennacchioni, *et al.*, 2006) settings of tonalitic psuedotachylite generation that we consider in this study.

Thickness displacement ratios, $w/\Delta\delta$ measured by Di Toro *et al.* (2005) and Di Toro, Hirose, Nielsen, Pennacchioni, *et al.* (2006) for pseudotachylite in tonalite within the Gole Larghe fault zone in the southern European Alps, exhumed from hypocentral depths of 9–11 km and T_0 of 250°C, are between 0.01 and 0.004. The associated calculated shear strengths are between 15 and 48 MPa, as depicted in Figure 1. This technique to estimate melt shear strength (equation 1c) was confirmed for normal stresses >20 MPa in experiments simulating coseismic slip on gabbro (Niemeijer *et al.*, 2011). In the field, the approach also requires some independent measure of the ambient temperature prior to the earthquake. Hypocentral temperature ($T_0 \approx 250$°C) of the Gole Larghe was estimated from deformation microstructures of quartz in cataclasites associated with the pseudotachylites, and by the mineral assemblage of coeval metamorphic alteration by Di Toro and Pennacchioni (2004).

Lab Observations of Melt Shear Strength

Meanwhile, advances in experimental design and technique (Tsutsumi and Shimamoto, 1997; Hirose and Shimamoto, 2003, 2005) and related theoretical developments (Di Toro, Hirose, Nielsen, and Shimamoto, 2006; Nielsen *et al.*, 2008, 2010) allow determination of the shear strength and constitutive response of friction melts of identical composition to the Gole Larghe fault-zone field exposures at a few to a few tens of MPa normal stress (Di Toro, Hirose, Nielsen,

Pennacchioni, *et al.*, 2006). Laboratory shear-melting experiments by Di Toro, Hirose, Nielsen, Pennacchioni, *et al.* (2006) were conducted at normal stresses between 5 and 20 MPa at a sliding velocity of 1.3 m/s for 4–8 s on the source tonalite collected from the Adamello batholith in the southern Italian Alps, from which the natural pseudotachylites were exhumed. In our study, the reported steady-state shear strengths from Di Toro, Hirose, Nielsen, Pennacchioni, *et al.* (2006) are assumed to be analogous to their natural equivalents. The melt steady-state shear strength resembles the unmelted strength of granitic faults (Byerlee, 1978) at the lowest normal stresses (Fig. 1) but is considerably weaker at 10–20 MPa normal stress, that is, the highest normal stresses tested. For extrapolation to the conditions of the natural pseudotachylites, the pressure dependence of fault strength $d\tau/d\sigma_e$ is the necessary metric; for these faults, shear strength increases very weakly with normal stress (0.05 MPa per MPa), and using this extrapolation from Di Toro, Hirose, Nielsen, Pennacchioni, *et al.* (2006), the implied natural strength at 9–11 km is less than 20 MPa (Fig. 1).

In this study, we examine the energy budget of earthquakes that generate shear melts of tonalitic composition. Knowing both the shear-generated heat from field observations and the shear strength from laboratory measurements puts constraints on energy partitioning that are lacking for all other earthquakes. Our approach is to use the laboratory and field measurements of coseismic fault strength along with the known static strength of the granitic host rock as the independent variables and determine the possible range of source parameters for the paleoearthquakes that generated these melts. Throughout the article, we refer to these prehistoric seismic events as earthquakes for simplicity. Particular goals are to establish whether these events could be consistent with typical earthquake source properties and what seismically observed properties may be diagnostic of melting. We find that earthquakes generating these pseudotachylites have atypical source properties that arise from the very high static frictional strength of granitic rock and the very low strength of shear melts. In this particular example, and likely in other rocks that have high frictional strengths at low sliding speed and for which shear heating produces a weak material (Di Toro, Han, *et al.*, 2011), the result is a large stress drop and relatively high radiated energy.

Energy during Dynamic Slip

Ignoring gravitational and rotational terms, the total energy of an earthquake E_T can be partitioned between heat Q_{all} and radiated energy E_s:

$$E_T = Q_{\text{all}} + E_s. \tag{2}$$

Here, as follows from the analysis of Savage and Wood (1971; e.g., McGarr, 1999; Beeler 2006), we have included in Q_{all} both the shear-generated heat that is available to be conducted away from the fault and also latent heats that are absorbed during shearing, for example, the heat of fusion (as in equation 1a; Di Toro *et al.*, 2005), heat of reaction during other phase changes (e.g., devolitalization, Brantut *et al.*, 2011), and the creation of surface energy that results from wear and comminution (Lachenbruch and Sass, 1980). The average shear stress on the fault is related to the total work $\bar{\tau} = E_T/A\Delta\delta$. Following the definition of heat above (equation 1b), we define a shear strength $\hat{\tau} = Q_{\text{all}}/A\Delta\delta$, $\hat{\tau}$ as the stress measure of energy dissipated and stored in the source, spatially and slip-averaged over the entire source region (McGarr, 1999; Beeler, 2006). It is a representative sliding strength of the fault, associated with energy distributed within the source, including shear-generated heat and latent heat associated with chemical reactions and the creation of surface energy. Using the standard definition of apparent stress, as the stress measure of radiated energy $\tau_a = E_s/A\Delta\delta$, the balance (equation 2) can be rewritten in stress units as

$$\bar{\tau} = \hat{\tau} + \tau_a, \tag{3}$$

(Savage and Wood, 1971; McGarr, 1994). The energy budget can be graphically expressed using a stress versus displacement diagram (Fig. 2; McGarr, 1994). The figure presents the definitions of stress quantities used throughout this article. In particular, the average stress is the difference between the static stress levels before and after the earthquake $\bar{\tau} = (\tau_0 + \tau_1)/2$, in which τ_0 is the initial stress on the fault prior to the earthquake and τ_1 is the stress after seismic slip.

Equating the shear strength that produces melt (equation 1b), to this stress measure of all the energy that is not radiated $\hat{\tau} = \hat{\tau}_m$, is the first crucial assumption in our analysis. Making this assumption presumes, for example, that any off-fault damage makes a negligible contribution to the energy budget. This is an assumption that is difficult

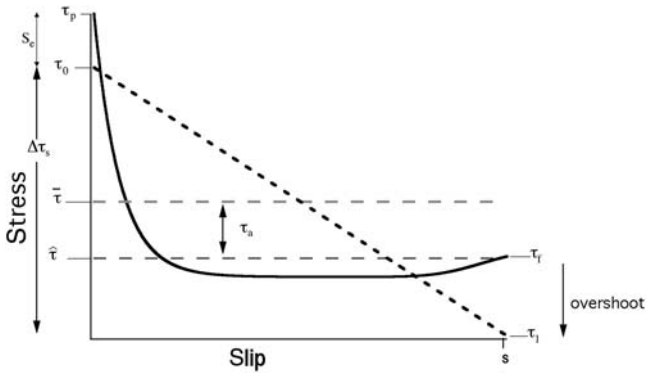

Figure 2. Earthquake stress versus slip diagram after McGarr (1994). Fault strength is shown as the heavy black line, whereas shear stress is the heavy black dashed line between τ_0 and τ_1, the starting and ending stresses. The average stress $\bar{\tau}$ is denoted by the heavy gray dashed line and the average fault strength $\hat{\tau}$ by the gray dashed line. The apparent stress is the difference between these lines. This example is a case of overshoot (Savage and Wood, 1971), where the final stress is less than the average strength. This is also a case where the starting stress is lower than the failure strength τ_p, defining a strength excess S_e.

to verify (Pittarello *et al.*, 2008) and not without associated controversy (e.g., Chester *et al.*, 2005; Wilson *et al.*, 2005; Ma *et al.*, 2006). Some of the limitations and implications, if this assumption is relaxed, are detailed in the Discussion section. Recent field studies of pseudotachylite (e.g., Di Toro, Hirose, Nielsen, Pennacchioni, *et al.*, 2006) have equated the fault shear strength $\hat{\tau}$ inferred from thickness–displacement ratios (equation 1c; Fig. 1) with the average crustal shear stress $\bar{\tau}$. The average shear strength and the static shear stress are approximately equivalent under special circumstances, as noted by McGarr (1994, 1999). This analysis to recover shear stress has been repeated elsewhere (e.g., Barker, 2005; Ujiie *et al.*, 2007; Andersen *et al.*, 2008; Billi and Di Toro, 2008). That relationship is valid only if $\hat{\tau} = \hat{\tau}_m$, as we have assumed, and if the apparent stress τ_a is relatively small. For shear melting, there are no published proportions of radiated energy and heat from laboratory measurements. There is also little knowledge of partitioning between heat and radiated energy from seismology or field relations; however, combining lab and field studies for granitic rock and considering the source properties of earthquakes observed seismically, the possible range of energy partitioning for shear-melted granitic faults can be addressed as we show next.

Earthquakes show a wide range of relationships between shear strength and shear stress during rupture. The difference can be parameterized to some degree by the slip overshoot

$$\xi = \frac{\hat{\tau} - \tau_1}{\Delta\tau_s} \tag{4}$$

(Savage and Wood, 1971; McGarr, 1994), in which $\Delta\tau_s$ is the static stress drop, the difference between the initial and final stresses (Fig. 2). Throughout the following analysis, we take the initial stress to be approximately equal to the static fault strength; this is the second crucial assumption. This is controversial, especially for plate boundary-scale faulting (Lapusta and Rice, 2003; Noda *et al.*, 2009). The assumption also differs from the general example in Figure 2 where the initial stress is lower than the static fault strength (the peak strength τ_p in Fig. 2). Such differences and the implications when this assumption is relaxed are dealt with in the Discussion section.

The static strength of the andesitic and granitiod rocks of the motivating studies of Sibson (1975) and Di Toro *et al.* (2005) follow Byerlee's law approximately (Byerlee, 1978; Fig. 1). To estimate the stresses at depth, we use guidance from the field studies of Di Toro and Pennacchioni (2004), Di Toro, Hirose, Nielsen, Pennacchioni, *et al.* (2006), and Di Toro, Hirose, Nielsen, and Shimamoto (2006) who used Andersonian assumptions for strike-slip faulting (Anderson, 1951). We use the mean depth of 10 km and a lithostatic stress gradient of 26 MPa/km, assume that the intermediate principal stress is equal to the mean stress and then average the results for hydrostatic pore pressure and dry conditions. The details of the estimate are in the Appendix. The effective normal stress is 122 MPa resulting in an initial stress of $\tau_0 = 104$ MPa for a Byerlee friction of 0.85. According to the regression of Di Toro, Hirose, Nielsen, Pennacchioni, *et al.* (2006) and Di Toro, Hirose, Nielsen, and Shimamoto (2006) at 10 km depth, the average dynamic strength is $\hat{\tau} = 10.6$ MPa. This coseismic shear strength is lower than the mean value inferred from the field study, $\hat{\tau} = 26.8$ MPa. Here and throughout, we report stress estimates to the tenths of MPa. This choice should not be interpreted as the accuracy of the estimate, which is unlikely to exceed a few MPa. However, we are interested in seismologic stress measurements, particularly stress drop, which can often be two to three orders of magnitude smaller than the above-quoted initial stress (see the subsequent Fig. 3). As a consequence, the apparent accuracy of stresses in this

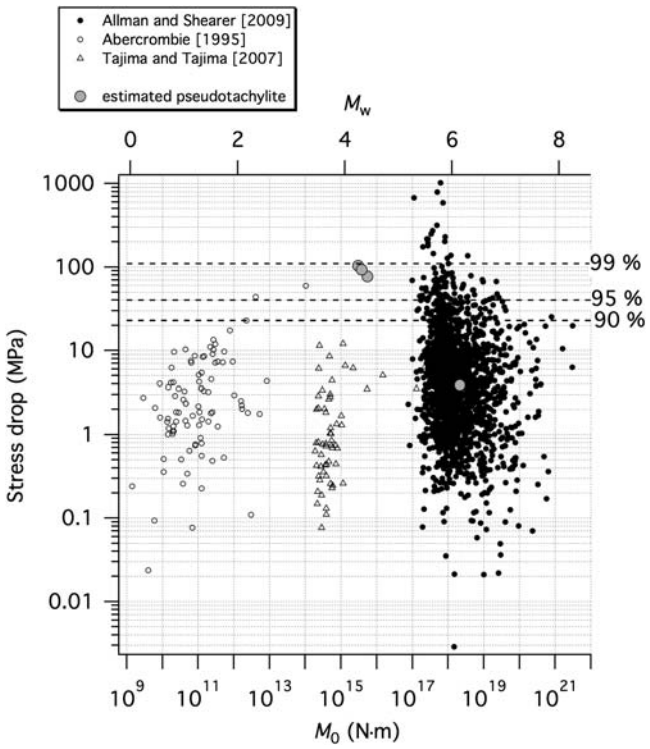

Figure 3. Variation of stress drop with seismic moment. Stress drops are from the previous studies of Abercrombie (1995), Tajima and Tajima (2007), and Allmann and Shearer (2009). Here, all stress drops are calculated using the Madariaga (1976) model. In the case of Tajima and Tajima (2007), the stress drops were calculated using their tabled moment and corner frequency f_c, using $\Delta\tau = M_0(f_c/0.42\beta)^3$ and $\beta = 3.9$ km/s, assuming rupture propagation at 0.9β, as in Allmann and Shearer (2009). An implication of these and other compilations (e.g., Hanks, 1977; Baltay *et al.*, 2011) is that stress drop is moment independent. The dashed lines are the 99%, 95%, and 90% boundaries from the global dataset of Allmann and Shearer (2009; solid circles). For example, 1% of the stress drops are larger than the 99% line (110 MPa). The 95% and 90% lines are stress drops of 40.3 and 22.9 MPa, respectively. Stress drops from exhumed pseudotachylite for the scenarios listed in Table 1 are shown in gray. Moment is calculated assuming a circular rupture, equation (6) in the text, a shear modulus $\mu = 30{,}000$ MPa, the average slip from the exhumed pseudotachylite (0.59 m), and the stress drops for each scenario (Table 1; see the Energy during Dynamic Slip section).

Table 1
Possible Earthquake Source Properties for Shear Melting at 10 km Depth, Effective Normal Stress = 122 MPa and Initial Stress of 104 MPa

Scenario	Average Strength, $\hat{\tau}$ (MPa)	Static Stress Drop, $\Delta\tau_s = \tau_0 - \tau_1$ (MPa)	Apparent Stress, τ_a (MPa)	Average Stress, $\bar{\tau} = \hat{\tau} + \tau_a$ $\bar{\tau} = (\tau_0 + \tau_1)/2$ (MPa)	Overshoot, $\xi = 0.5 - \tau_a/\Delta\tau_s$	Seismic Efficiency, $\eta = \tau_a/\bar{\tau}$	Thermal Efficiency, $\hat{\tau}/\bar{\tau}$	r (m)	A(m^2)	Moment (N·m)
Orowan $\hat{\tau} = \tau_1$	**26.8**	77.2	38.6	65.4	**0**	0.59	0.41	314	3.1×10^5	5.5×10^{15}
Complete stress drop $\Delta\tau_s = \tau_0$	**26.8**	**104**	25.2	52	0.26	0.48	0.52	233	1.7×10^5	3.0×10^{15}
Typical stress drop $\Delta\tau_s = 3.9$ MPa	**26.8**	**3.9**	75.3	102	−19.3	0.73	0.27	6224	1.2×10^8	2.1×10^{18}
Typical overshoot $\xi = 0.166$	**26.8**	93	30.7	57.5	**0.166**	0.53	0.47	261	2.1×10^5	3.8×10^{15}

Four scenarios are considered and source parameters are tabulated for an average shear strength of 26.8 MPa (field). For each scenario the assumed values are in bold. The values for the stress parameters can be derived directly from the initial and average strength, the definitions in the column headers, and the assumptions that are listed in the scenario rows, using the assumed (bold) table values.

report is required to estimate stress drop in our analyses. Typical stress drops are a few MPa and our reported stresses are to the order of 10%.

In the following, we consider four possible scenario earthquake source parameters for shear melting at this depth. The scenarios are intended to span the range of plausible seismically observed source properties. For all four scenarios, we calculate source parameters using the average field-measured shear strength of 26.8 MPa. These results are described in the following and listed in Table 1.

Scenario 1 is the Orowan condition where the stress drops exactly equal to the dynamic fault strength $\hat{\tau} = \tau_1$ (Orowan, 1960; Kanamori and Heaton, 2000), then $\Delta\tau_s = 77.2$ MPa, the overshoot (equation 4) is zero, $\bar{\tau} = 65.4$ MPa and $\tau_a = 38.6$ MPa. This would be a case of high seismic efficiency relative to that which has been assumed for pseudotachylite (Di Toro, Hirose, Nielsen, Pennacchioni, *et al.*, 2006), $\eta = \tau_a/\bar{\tau} = 0.59$; 59% of the total energy would be radiated. Because the Orowan condition is the most often used assumption in studies of the earthquake energy budget such as in a number of seminal contributions, compilations, and reviews (e.g., Kanamori and Heaton, 2000; Kanamori and Brodsky, 2004; Venkataraman and Kanamori, 2004; Abercrombie and Rice, 2005; Viesca and Garagash, 2015), it is useful for placing estimated source parameters and their uncertainty in context. For example, had we used the upper limit of the field estimated fault strength (48 MPa) rather than the average, the resulting seismic efficiency of 37% would still be much higher than typical seismological estimates (e.g., Wyss, 1970; McGarr, 1999).

Scenario 2 is a complete stress drop, then, $\bar{\tau} = 52$ MPa, $\xi = 0.26$, and $\tau_a = 25$ MPa, again, a case of high seismic efficiency $\eta = \tau_a/\bar{\tau} = 0.48$.

Both scenarios 1 and 2 would be out of the range of typical earthquake source properties, as follows.

In the following analysis, we use the stress drops of a recent global compilation (Allmann and Shearer, 2009) for reference. These are determined from seismically inferred corner frequencies (f_c) using the Madariaga source model (Madariaga, 1976). Because stress drops depend on $(f_c/C)^3$, in which C is a model-dependent scalar, small differences in the scalar (model) produce much larger differences in stress drop, up to a factor of 5.5 (e.g., Kaneko and Shearer, 2014). Thus, constraints on source properties from stress drop are weak. Specific differences between models and the difficulties that arise in using stress drop in studies of source physics are discussed in the Stress Drop and the Choice of Source Model section. Typical values of stress drop are a few MPa, albeit with significant logarithmic variability (Fig. 3, after Allmann and Shearer, 2009). The dashed lines that are superimposed mark 99%, 95%, and 90% of the stress drops in the Allmann and Shearer dataset. For instance, 1% of the earthquakes have stress drops larger than the 99% line, and so on. The 99%, 95%, and 90% lines are associated with stress drops of 110, 40, and 23 MPa, respectively. Stress drops as large as those in scenarios 1 and 2 are found only in a few percent or less of natural earthquakes. This apparent inconsistency between seismologically inferred values of MPa static stress drop and the ∼77 MPa dynamic stress drop from the field and extrapolated from laboratory observations of melting (Fig. 1) is a paradox long expected from theoretical considerations of shear heating (Sibson, 1975; Lachenbruch, 1980; Rice, 2006; Noda *et al.*, 2009). Similar but potentially stronger constraints on source properties come from apparent stress because it is not model dependent. In comparison with the scenario estimates of apparent stress, Figure 4 shows apparent stresses compiled by Baltay *et al.* (2010). The estimated apparent stresses using Orowan's (scenario 1) and the complete stress drop (scenario 2) assumptions are outside the range of these seismic observations that lie between 0.1 and 10 MPa (Fig. 4).

We also consider the implied overshoot of these scenarios (Table 1). The energy balance with stress as the dependent variable (equation 3) can be rewritten in terms of stress drop, overshoot, and apparent stress as

$$\frac{\tau_a}{\Delta\tau_s} = 0.5 - \xi \tag{5}$$

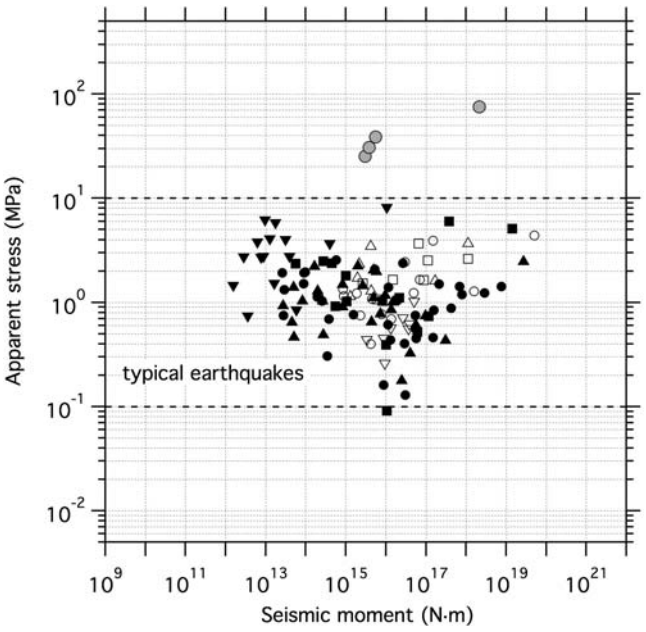

Figure 4. Variation of apparent stress with seismic moment. Compilation of apparent stress (right axis) from Baltay *et al.* (2010, 2011). The dashed lines are for 10 and 0.1 MPa and are the approximate bounds on the observations. The implication of this and other compilations (e.g., Ide and Beroza, 2001) is that apparent stress is moment independent. Apparent stresses for exhumed pseudotachylite for the scenarios listed in Table 1 are plotted in gray. Seismic moments for the pseudotachylite are calculated as described in the caption of Figure 3.

(Savage and Wood, 1971; McGarr, 1994, 1999). Keep in mind that the model dependence of stress drop means that bounds on overshoot are dependent on the choice of source model; for all the standard source models, stress drop tends to be a fixed factor of apparent stress (e.g., Singh and Ordaz, 1994; Kaneko and Shearer, 2014). Because both stress drop (Hanks, 1977) and apparent stress (Ide and Beroza, 2001) are arguably magnitude independent, earthquake overshoot is also magnitude independent according to equation (5). For the Madariaga model at 0.9β, slip overshoots the static value by 20% (Madariaga, 1976), which corresponds to a stress measure of overshoot (equation 4) of 0.17, which is not so different from scenario 2. Because they involve restrictions on stress drop, with the exception of overshoot, the source parameters from scenarios 1 and 2 are independent of the choice of source model; this is not the case for scenarios 3 and 4 that follow.

Scenario 3 is typical stress drop. Instead of complete stress drop or Orowan's assumption, it takes the stress drop to be $\Delta\tau_s = 3.8$ MPa, then, $\bar{\tau} = 102$ MPa, $\xi = -19.3$, and $\tau_a = 75$ MPa. This would be a case of extreme undershoot, undershoot larger than can be inferred from seismic observations (see analysis of data of Venkataraman and Kanamori, 2004, in Beeler, 2006), and again, high seismic efficiency $\eta = \tau_a/\bar{\tau} = 0.73$.

Scenario 4 is typical overshoot, $\xi = 0.17$, leading to $\Delta\tau_s = 93$ MPa, $\bar{\tau} = 57.5$ MPa, and $\tau_a = 30.7$ MPa; this too would be a case of high seismic efficiency $\eta = \tau_a/\bar{\tau} = 0.53$.

To put the scenarios in context with seismological observations, they are plotted versus seismic moment in Figures 3 and 4 by assuming a circular rupture. Using the average slip from the exhumed pseudotachylites of 0.59 m (Di Toro, Hirose, Nielsen, Pennacchioni, *et al.*, 2006; Di Toro, Hirose, Nielsen, and Shimamoto, 2006) and the stress drops from Table 1, we can calculate the radius

$$r = \frac{7\pi\mu\Delta\delta}{16\Delta\tau_s} \tag{6}$$

(area $A = \pi r^2$ and seismic moment $M_0 = \mu A\Delta\delta$, Table 1). For all scenarios the apparent stress is outside the typical values. All the stress drops, except for the case where a typical value was assumed, are in the upper few percent of the observations. More extreme earthquake source properties result if the lab-inferred value of the melt shear strength is used, instead of the field values.

Discussion

Partitioning of radiated and thermal energy during earthquake slip might be most easily considered by normalizing equation (3) by the average stress, defining a total thermal efficiency:

$$\frac{\hat{\tau}}{\bar{\tau}} = 1 - \eta, \tag{7}$$

the ratio of the average dynamic shear strength to the average coseismic shear stress, in which η is the seismic efficiency as defined above. As noted by McGarr (1994, 1999), for dynamic rupture controlled by low-temperature friction at very small displacements, the thermal efficiency is high, for example, greater than 90% (Lockner and Okubo, 1983), and the seismic efficiency is less than 10%. However, for much more extreme dynamic weakening such as seen for shear melts with low-dynamic shear strength, so long as the initial stress is high, the seismic efficiency must be significantly larger than it is in low-temperature friction experiments.

In this context, we can draw a number of conclusions about earthquake source properties associated with the pseudotachylites. Based on our four scenarios, we expect that radiated energy will be similar to or exceed shear heating during the earthquake-generated formation of natural shear melts; equivalently, the seismic efficiency is similar to or exceeds the thermal efficiency. A related conclusion is that because the radiated energy is large, from equation (3), fault shear stress during earthquakes cannot be estimated from exhumed pseudotachylite; the estimates from previous studies assumed negligible radiated energy and directly equated shear stress with the field-measured strength. Thus, the estimates from prior studies are likely an implausible lower bound on the shear stress, and, if so, the field studies of exhumed pseudotachylite have underestimated stress. The degree that stress differs from strength depends on how much

the slip overshoots (or undershoots) the value that would result from the dynamic stress drop alone (the difference between the final stress and the shear strength) and also on the strength excess (how much the failure strength of the fault exceeds the initial stress, see the discussion below). Our calculations suggest underestimation by 1.9–2.8 times. Overshoot is not determined in the existing shear-melting laboratory experiments but it is an active target for laboratory investigation (e.g., Sone and Shimamoto, 2009; Di Toro, Nielsen, *et al.*, 2011). Overshoot might reasonably be inferred from careful measurement in subsequent tests or in relatively simple calculations of dynamic shear melting. According to this analysis, earthquakes that produce pseudotachylite are outside the range of seismic observations of apparent stress (Fig. 4).

Reconciling the Energy Balance

There are, however, a number of ways in which our energy accounting may have gone astray. Much uncertainty in our balance is associated with the choice of a Madariaga source model that has the largest stress drop of the conventional models. Still, had we used a dataset in which the stress drops were determined using the Brune model that has the lowest stress drops, apparent stress still would be out of the bounds of the Baltay *et al.* (2010) dataset in all four scenarios, and the discrepancy between the predicted and observed stress drops would be even larger. As above, while acknowledging that the choice of source model has first-order implications for earthquake source properties, source model choice does not affect our conclusion that the presence of pseudotachylite implies an unusual earthquake source. Additional discussion of source models is found in the Stress Drop and the Choice of Source Model section.

We now consider whether relaxing the two critical assumptions about initial stress and dissipated energy may allow shear melting to produce more typical earthquake source properties. First, we assumed that the heat inferred from pseudotachylite is equivalent to all energy that does not go into the radiated field (i.e., $\hat{\tau} = \hat{\tau}_m$). This ignores any off-fault damage that may be generated during rupture, such as brittle failure associated with stress concentrations about the tip of the propagating rupture (Andrews, 1976, 2005) or from slip on rough fault surfaces (Chester and Chester, 2000; Dieterich and Smith, 2009; Dunham *et al.*, 2011). Such energy is most often partitioned into a shear fracture energy term in an expanded energy balance (e.g., Tinti *et al.*, 2005). Fracture energy is heat and latent-heat, the energy that goes into the creation of shear and tensile fracture surfaces and into slip on shear fractures in the damage zone about the rupture (Ida, 1972; Andrews, 1976). In well-posed dynamic rupture models, it is the portion of this energy associated with inelastic deformation about the tip of the rupture that limits the propagation speed (Andrews, 1976, 2005). Andrews (2005) has further shown that the size of this energy contribution scales with the dynamic stress drop, thus mechanisms that produce large strength losses, such as shear melting, implicitly require some compensation in off-fault fracture energy as well as in radiation.

Second, we assumed up to this point that the initial stress is approximately equal to the static fault strength which, in the case of the felsic crystalline rocks of the motivating studies, implies high initial stress in the crust. If instead we assume that the initial stress is lower than the failure stress, as depicted in the schematic of Figure 2, there is a strength excess S_e defined by the difference between the failure strength and the initial stress (Andrews, 1985). Such an excess arises naturally in regions with strength or stress heterogeneity. For example, imagine a fault surface that on average is strong but has a limited contiguous region of weak material. If the incipient rupture starts in that weak area, and that region is sufficiently large and slips far enough to raise the stress on the adjacent portion of the strong region to its failure stress, then an earthquake rupture can occur at a lower stress than the average failure strength of the fault.

To relax both critical assumptions about initial stress and dissipated energy, we modify equation (3). To consider contributions of damage to source properties, it is convenient to use a stress measure of fracture energy. Fracture energy G_e has the dimensions of energy per unit area, so the fracture stress then is the fracture energy divided by the total slip, $\tau_c = G_e/\Delta\delta$. Replace the shear resistance in equation (3) with the sum of that which goes into shear heat and that which resides in fracture energy, $\hat{\tau} = \hat{\tau}_m + \tau_c$. To incorporate the strength excess, we replace the average stress in equation (3) with $\tau_0 - \Delta\tau_s/2$ and replace the initial stress with $\tau_p - S_e$. Making these substitutions, the balance (equation 3) becomes

$$\tau_c + S_e = \tau_p - \frac{\Delta\tau_s}{2} - \tau_a - \hat{\tau}_m. \tag{8a}$$

Implementing equation (8a) for pseudotachylite, $\tau_p =$ 104 MPa and $\hat{\tau}_m = 26.8$ MPa. To produce a stress drop within the 95% bound and apparent stresses to be at the upper limit of the observations, corresponding to $\Delta\tau_s = 40$ and $\tau_a = 10$ MPa, respectively, equation (8a) is

$$\tau_c + S_e = 47.2 \text{ MPa}. \tag{8b}$$

Fracture Energy

If the right side of equation (8b) were all due to fracture energy ($S_e = 0$), the fracture stress would exceed the stress drop. For comparison with typical observations, a measure of the associated efficiency is the ratio of fracture energy times the fault area to the energy associated with the stress drop: $\eta_c = G_e/\Delta\tau_s\Delta\delta$; equivalently, the ratio of the fracture stress to the stress drop: $\eta_c = \tau_c/\Delta\tau_s$. Beeler *et al.* (2012) compiled some limited and model-dependent data on this efficiency from Abercrombie and Rice (2005) and found no natural values greater than 0.5. The minimum fracture

efficiency to bring the pseudotachylite data in line with typical earthquakes is 1.2. However, as none of the prior estimates of fracture stress or efficiency strictly include off-fault damage or consider the impact of roughness on fracture energy, these remain topics for further research.

The Strength Excess and Fault Roughness

Consider instead that all of the right side of equation (8b) were from the strength excess ($\tau_c = 0$); then the difference between the initial stress and the failure strength would be ~47 MPa. In that case, the heterogeneity would have to be quite high in association with these earthquakes in crystalline rock. Because the source region is a batholith and arguably not highly heterogeneous in elastic or friction properties, we can only appeal to stress heterogeneity to produce the necessary strength excess. Some insight into the allowable amplitude of stress heterogeneity may be found in studies of roughness contributions to shear strength (Chester and Chester, 2000; Dieterich and Smith, 2009; Dunham *et al.*, 2011; Fang and Dunham, 2013). The idea is that fault shear resistance consists of two components: the shear resistance due to frictional slip on a planar fault surface, and that which results from fault roughness. Based on measurements of natural fault roughness, the amplitude to wavelength ratio α appropriate for faults that host intermediate-sized earthquakes is between 10^{-3} and 10^{-2} (Power and Tullis, 1991; Sagy *et al.*, 2007). According to the modeled estimates to date, the upper end of this range produces dramatic stress heterogeneity on the fault and significant additional shear strength beyond the interface friction (Chester and Chester, 2000; Dieterich and Smith, 2009), deemed roughness drag τ_{drag} by Fang and Dunham (2013). How roughness may define the strength excess would be to allow earthquake nucleation on relatively flat portions of the fault at stress levels equal to the frictional strength.

Because roughness drag increases the shear heating above that is associated with slip on planar surfaces with the same frictional strength (Griffith *et al.*, 2010), this contribution is included in the pseudotachylite-estimated coseismic shear strength (equation 1b). Drag may be used to explain the difference between lab- and field-measured values of shear strength. Formally,

$$\tau_{\text{drag}} = \frac{8\pi^3 \alpha^2 G' \Delta\delta}{\lambda_{\text{min}}}, \tag{9}$$

in which λ_{min} is the minimum wavelength of the roughness and G' is the shear modulus divided by 1 minus Poisson's ratio (Fang and Duham, 2013). Taking the ratio of slip to λ_{min} to be of order 1 (Fang and Dunham, 2013), the amplitude ratio is $\alpha = \sqrt{\tau_{\text{drag}}/G' 8\pi^3}$. Assuming the difference between the lab and field shear strengths (~16 MPa) is the dynamic roughness drag, and $G' = 40$ GPa, then $\alpha = 0.0013$.

The roughness drag as estimated by Fang and Dunham (2013; equation 9) and in the prior study by Dieterich and Smith (2009) is calculated for a discontinuity in otherwise intact rock, assuming a small amount fault slip relative to the smallest wavelength of roughness, elastic stress transfer, and no dilatancy. Results of these assumptions are that the roughness drag is not pressure dependent and it does not depend on the absolute level of the differential stress. As such, the same roughness drag applies to both the sliding and failure strengths at all depths, so long as the amplitude and characteristics of the roughness are not changed substantially by slip or by ambient stress levels. Accordingly, our estimated value of 16 MPa inferred from sliding is also the strength excess due to fault roughness-generated stress heterogeneity. Even if we allow that our failure strength of 104 MPa is overestimated by 16 MPa, that is not enough of a strength excess to bring the pseudotachylite source properties in line with more typical earthquakes.

Admittedly these estimates do not consider contributions from material heterogeneity; nonetheless those should be small in the relatively homogeneous source region of the pseudotachylite. Contributions from slip heterogeneity are also not considered. Because those will correlate with fault roughness in a homogeneous material (Dunham *et al.*, 2011; Fang and Dunham, 2013), we expect that the difference between our estimate and the needed value of 47 MPa precludes reconciling the observations and typical earthquake source properties with this model of the strength excess. Nonetheless, given that our roughness estimate is based entirely on the difference between field and lab-melt shear strengths, along with the large uncertainties associated with the field-inferred strength, and our assumption of the high Byerlee failure strength, the strength excess remains perhaps the most poorly constrained of all the poorly constrained earthquake source properties.

To assess whether the combined effects of strength excess and fracture energy are sufficient to bring pseudotachylite in line with typical earthquakes, use the strength excess of 16 MPa in equation (8b) to reduce the needed fracture stress from 47 to 31 MPa. The associated minimum fracture efficiency would be ~0.8, exceeding the limited observations (Abercrombie and Rice, 2005) by a factor of 1.5. Again, we conclude that seismically generated pseudotachylite requires atypical earthquake source properties, a result that seems robust even when limitations of the assumptions are taken into account.

Future Work on Fault Roughness

There are physical limits on the estimate of roughness drag in equation (9). The underlying theory breaks down at high but realistic amplitude ratios (Dieterich and Smith, 2009; Fang and Duhnam, 2013), especially at near-surface and intermediate depths. For example, at a modest effective normal stress of 100 MPa, the strength of intact granite is about 150 MPa, whereas the frictional strength is about 85 MPa. From equation (9), using the same slip and elastic assumptions as previously, the roughness drag of a fault at

the upper end of the natural amplitude ratio range, $\alpha = 0.01$, is 990 MPa, more than ten times the frictional strength and approximately six times the intact rock strength. Empirically, this is out of bounds and arises mostly because the estimate forbids the dilatancy that limits rock and fault strength in the first place (Brace *et al.*, 1966; Escartin *et al.*, 1997). Similarly, at more modest values of the amplitude ratio but at greater depth where the normal stress is high, according to equation (9), friction will dominate the shear resistance, as friction increases with normal stress whereas the roughness contribution does not. This is hard to reconcile with existing laboratory data in which both sliding friction and intact rock strength increase with confining pressure. In practice, many of these issues with equation (9) are dealt with in numerical fault models (Fang and Dunham, 2013). There, the stresses that arise from slip on rough surfaces are calculated incrementally with slip (rather than assuming that $\Delta\delta/\lambda_{\min} = 1$) and when the drag stress reaches the failure strength of surrounding rock the material yields via a separate pressure-dependent plasticity relation.

Simpler models of rough faults and the bounds on the resulting stress heterogeneity might be constructed using existing laboratory data. Among the nonphysical aspects of the underlying theory (equation 9) are lack of dilatancy and the fault is zero thickness and fully localized resulting in a stationary shear zone. On the latter, natural fault zones have finite thickness that likely provides some degree of freedom to deform internally in order to accommodate roughness of the fault-bounding rock. On the former, disallowing rigid and fracture dilatancy on a fault between rock surfaces is contrary to the most basic physical observations of brittle deformation and frictional slip (e.g., Brace *et al.*, 1966; Marone *et al.*, 1990). Because of these issues, we suggest that the contribution of roughness to fault shear resistance is inherently pressure dependent, such that it is smaller than equation (9) at near-surface conditions where, in the presence of very low normal stress and distributed shear, roughness likely leads to rigid dilation rather than damage in the surrounding rock, and so that the contribution from roughness does not diminish relative to friction at elevated confining pressure. Furthermore, the roughness contribution is bounded by existing experimental data to be less than or equal to the strength of intact rock minus the frictional failure strength at the confining pressure and temperature of interest. Future experiments on faults with amplitude ratios between 0.01 and 0.001, at effective normal stresses and temperatures spanning those of the brittle crust should better establish the contributions of roughness to fault strength.

Stress Drop and the Choice of Source Model

Choice of source model has a very large effect on the inferred bounds of static stress drop such as the 95% bound $\Delta\tau_s = 40$ MPa from Allmann and Shearer (2009) that is superimposed on in Figure 3. The Madariaga source produces stress drops that are a factor of 2.6 larger than from the Sato and Hirasawa (1973) model and 5.5 times larger than Brune (1970). Decreasing the upper bound in Figure 3 to that which would be inferred from Brune (1970) would place all scenarios except scenario 3 further out of range of typical stress drops. This model dependency of static stress drop is a significant barrier to using stress drop as a metric in studies of source physics (McGarr, 1999). Although there is no strict constraint on stress drops from pseudotachylite, our analysis suggests that regardless of the source model used the stress drops from pseudotachylite are unusual for earthquakes.

There are, unfortunately, additional fundamental problems relating the stress drop from standard source models to pseudotachylite. For the Brune, Sato and Hirasawa, and Madariaga source models, the ratio of apparent stress to static stress drop is fixed with a value $0.22 < \tau_a/\Delta\tau_s < 0.4$. In other words, these are all crack-like rupture models that overshoot. In contrast, experimental measurements suggest that the shear melts show rapid coseismic strength recovery (Di Toro, Nielsen, *et al.*, 2011) that, when extrapolated to a propagating confined rupture, are more consistent with undershoot and pulse-like propagation. In the absence of a definitive earthquake source model that allows for undershoot or seismic methods that reliably distinguish undershoot from overshoot, it will remain difficult to use static stress drops to relate laboratory observations to earthquake seismology.

Source Properties of Shear Melts

The source parameters in scenarios 1–4 are perhaps the seismic corollary to the interpretation of the geologic record that pseudotachylite is rare (Sibson and Toy, 2006). Although the interpretation is not without controversy (Kirkpatrick *et al.*, 2009; Kirkpatrick and Rowe, 2013), the corollary is not unexpected. Although pseudotachylite is known to form under a wide range of conditions, for example, in the presence of fluids, in metamorphic terrains, and even in large events within melange (e.g., Bjørnerud, 2010, Meneghini *et al.*, 2010; Toy *et al.*, 2011), the friction-melting experiments of Di Toro, Hirose, Nielsen, Pennacchioni, *et al.* (2006) suggest that pseudotachylites are easily formed during imposed localized slip on precut faults in cohesive rocks that are dry. Many field studies also suggest that the typical ambient condition of pseudotachylite is the dry crystalline basement of the continental crust (Sibson and Toy, 2006), as is the case for most nappes in the western Alps, where pseudotachylites are not uncommon fault rocks (Pennacchioni *et al.*, 2006; Di Toro *et al.*, 2009). The higher stress-drop characteristics of intraplate earthquakes (Scholz *et al.*, 1986), including those of some very high stress-drop earthquakes (e.g., Viegas *et al.*, 2010; Ellsworth *et al.*, 2011) may indicate related properties of the source, once differences in source model are accounted for. Large stresses relative to the failure strength, large stress drops, and relatively low fault roughness may lead to some diagnostic rupture properties associated with pseudotachylite formation. High initial stress

levels promote a strong tendency for supershear rupture up to the compressional wavespeed, specifically when the ratio of the strength excess to the dynamic stress drop S is lower than 1.77 (Andrews, 1985), as claimed to be observed experimentally by Passelègue *et al.* (2013). Taking the 16 MPa strength excess, an initial stress of 104 MPa, and sliding strength of 26.8 MPa, Andrews' S ratio is no higher than 0.26 and supershear rupture is expected. A large stress drop, low roughness, and high initial stress may also tend to promote propagation as an expanding crack rather than as a slip pulse (Zheng and Rice, 1998).

An appealing third idea explaining the difference between typical earthquake stress drops and the ~77 MPa values inferred for pseudotachylite dynamic stress drops relaxes our implicit assumption that pseudotachylites are representative of the dynamic properties of the earthquakes that generated them. Sibson (2003) suggested that faults have significant spatially varying dynamic properties, allowing the majority of the shear strength to be concentrated in the regions of high geometric complexity (e.g., fault bends or stepovers). Fang and Dunham (2013) reached a similar conclusion when considering large ruptures. This kind of model, where part of the fault is dynamically weak but most of the shear strength is concentrated elsewhere, perhaps in relatively limited areas, is similar to the numerical fault models with heterogeneous stress conditions that allow fault slip at low-average stress levels (Lapusta and Rice, 2003; Noda *et al.*, 2009). Under the Sibson (2003) conceptual model, pseudotachylite is generated on parts of the fault that are geometrically simple prior to rupture, but it does not contribute significantly to the dynamic shear strength of the entire fault. Our scenario 3, where we have imposed a typical stress drop, is related to this kind of event. For scenario 3, the rupture dimension is much larger than the other scenarios, producing an **M** 6 earthquake. In any event, the Sibson model would remove the discrepancy between typical earthquake stress drops and the implied strength loss by pseudotachylite in granite rock and would allow pseudotachylite to be more common as advocated by Kirkpatrick and Rowe (2013). Meanwhile, the mechanical properties of pseudotachylite would be largely irrelevant to the average seismically inferred source properties, such as static stress drop and apparent stress. Testable implications of this model would be that during seismic slip the majority of shear-generated heat would be concentrated in distinct local regions of low stress drop. In cases where the stress is high, regions of low shear strength due to the formation of pseudotachylite would appear as asperities in seismic inversions where the stress drop and radiated energies are high (e.g., Kanamori, 1994; Bouchon, 1997; Kim and Dreger, 2008). A hope is that the character of radiated energy from such asperities could be quantitatively related to laboratory and field studies of fault properties and in some cases related to a particular shear deformation mechanism in the fault zone (e.g., melting, thermal pressurization). This would require particular mechanisms to have characteristic source properties, for example, a distinctive frequency content. Making such a link between various source properties and source mechanisms might be made using synthetic seismograms generated by spontaneous dynamic rupture simulations (e.g., Harris, 2004; Andrews, 2005), as developments in that field are directed specifically at the physics within the source (Harris *et al.*, 2009).

Conclusions

The analysis of the energy budget and source properties of pseudotachylite-generating intermediate-sized earthquakes of the Gole Larghe fault zone in the Italian Alps where the dynamic shear strength is well constrained by field and laboratory measurements suggests that these earthquakes have unusual source parameters. The assumptions are that seismically determined corner frequency relates to stress drop by the Madariaga (1976) relation, that the heat inferred from pseudotachylite thickness and fault displacement is equivalent to all energy that does not go into the radiated field, and that the initial stress is approximately equal to the static fault strength. For the felsic crystalline rocks of the source region, the final assumption results in an initial shear stress on the order of 100 MPa. Stress drops and apparent stress are larger than a few tens of MPa, unlike typical earthquakes, and the radiated energy equals or exceeds the shear-generated heat. Relaxing these assumptions, the observations still cannot be reconciled with typical earthquake source properties unless fracture energy is routinely significantly greater than in existing models, pseudotachylite is not representative of average fault shear strength during the earthquake that generated it, or the strength excess is larger than we have allowed.

Data and Resources

All data used in this article came from published sources listed in the references.

Acknowledgments

This article was greatly improved by U.S. Geological Survey (USGS) internal reviews of Annemarie Baltay and Greg McLaskey, and particularly by journal reviews from Emily Brodsky and Virginia Toy. N. M. B. thanks Art McGarr, Alan Rempel, Tom Hanks, Annemarie Baltay, Eric Dunham, Yoshi Kaneko, and Rachel Abercrombie for guidance in understanding shear melting and empirical, model-dependent, and theoretical limits on earthquake source properties. Much of the analysis was developed for an experimental study of shear melting with David Lockner, Diane Moore, and Brian Kilgore. Funding for G. D. T., S. N., and N. M. B. was provided by European Union European Research Council Project 205172, "Uncovering the Secrets of an Earthquake: Multidisciplinary Study of Physico-Chemical Processes During the Seismic Cycle," and European Research Council Project 614705, "New Outlook on seismic faults: From Earthquake nucleation to arrest".

References

Abercrombie, R. E. (1995). Earthquake source scaling relationships from –1 to 5 ML using seismograms recorded at 2.5 km depth, *J. Geophys. Res.* **100,** 24,015–24,036.

Abercrombie, R. E., and J. R. Rice (2005). Can observations of earthquake scaling constrain slip weakening, *Geophys. J. Int.* **162,** 406–424.

Allmann, B. B., and P. M. Shearer (2009). Global variations of stress drop for moderate to large earthquakes, *J. Geophys. Res.* **114,** no. B1, doi: 10.1029/2008JB005821.

Andersen, T. B., K. Mair, H. Austrheim, Y. Y. Podladchikov, and J. C. Vrijmoed (2008). Stress release in exhumed intermediate and deep earthquakes determined from ultramafic pseudotachylite, *Geology* **36,** 995–998.

Anderson, E. M. (1951). *The Dynamics of Faulting and Dyke Formation with Application to Britain*, Oliver and Boyd, White Plains, New York, 206 pp.

Andrews, D. J. (1976). Rupture propagation with finite stress in anti-plane strain, *J. Geophys. Res.* **18,** 3575–3582.

Andrews, D. J. (1985). Dynamic plane-strain shear rupture with a slip-weakening friction law calculated by a boundary integral method, *Bull. Seismol. Soc. Am.* **75,** 1–21.

Andrews, D. J. (2005). Rupture dynamics with energy loss outside the slip zone, *J. Geophys. Res.* **110,** no. B1, doi: 10.1029/2004JB003191.

Baltay, A., S. Ide, G. A. Prieto, and G. C. Beroza (2011). Variability in earthquake stress drop and apparent stress, *Geophys. Res. Lett.* **38,** L06303, doi: 10.1029/2011GL046698.

Baltay, A., G. Prieto, and G. C. Beroza (2010). Radiated seismic energy from coda measurements indicates no scaling in apparent stress with seismic moment, *J. Geophys. Res.* **115,** no. B08314, doi: 10.1029/2009JB006736.

Barker, S. L. L. (2005). Pseudotachylyte-generating faults in Central Otago, New Zealand, *Tectonophysics* **397,** 211–223.

Beeler, N. M. (2006). Inferring earthquake source properties from laboratory observations and the scope of lab contributions to source physics, in *Earthquakes: Radiated Energy and Earthquake Physics*, R. Abercrombie, A. McGarr, H. Kanamori, and G. Di Toro (Editors), Geophysical Monograph Series 170, American Geophysical Union, Washington, D. C., 99–119.

Beeler, N. M., B. Kilgore, A. McGarr, J. Fletcher, J. Evans, and S. R. Baker (2012). Observed source parameters for dynamic rupture with non-uniform initial stress and relatively high fracture energy, in *Physico-Chemical Processes in Seismic Faults*, G. Di Toro, F. Ferri, T. Mitchell, S. Mittempergher, and G. Pennacchioni (Editors), *J. Struct. Geol.* 38, 77–89.

Billi, A., and G. Di Toro (2008). Fault-related carbonate rocks and earthquake indicators: Recent advances and future trends, in *Structural Geology: New Research*, S. J. Landowe and G. M. Hammlerp (Editors), Nova Publishing, New York, 63–86.

Bjørnerud, M. (2010). Rethinking conditions necessary for pseudotachylyte formation: Observations from the Otago schists, South Island, New Zealand, *Tectonophysics* **490,** 69–80, doi: 10.1016/j.tecto.2010.04.028.

Bouchon, M. (1997). The state of stress on some faults of the San Andreas system as inferred from near-field strong motion data, *J. Geophys. Res.* **102,** 11,731–11,744, doi: 10.1029/97JB00623.

Brace, W. F., B. W. Paulding, and C. H. Scholz (1966). Dilatancy in the fracture of crystalline rock, *J. Geophys. Res.* **71,** 3939–3953.

Brantut, N., R. Han, T. Shimamoto, N. Findling, and A. Schubel (2011). Fast slip with inhibited temperature rise due to mineral dehydration: Evidence from experiments on gypsum, *Geology* **39,** 59–62.

Brune, J. N. (1970). Tectonic stress and the spectra of seismic shear waves from earthquakes, *J. Geophys. Res.* **75,** 4997–5009.

Byerlee, J. D. (1978). Friction of rocks, *Pure Appl. Geophys.* **116,** 615–626.

Chester, F. M., and J. S. Chester (2000). Stress and deformation along wavy frictional faults, *J. Geophys. Res.* **105,** no. B10, 23,421–23,430, doi: 10.1029/2000JB900241.

Chester, J. S., F. M. Chester, and A. K. Kronenberg (2005). Fracture surface energy of the Punchbowl fault, San Andreas system, *Nature* **437,** 133–136.

Dieterich, J. H., and D. E. Smith (2009). Nonplanar faults: Mechanics of slip and off-fault damage, *Pure Appl. Geophys.* **166,** 1799–1815.

Di Toro, G., and G. Pennacchioni (2004). Super-heated friction-induced melts in zoned pseudotachylytes with the Adamello tonalites (Italian southern Alps), *J. Struct. Geol.* **26,** 1783–1801.

Di Toro, G., R. Han, T. Hirose, N. De Paola, K. Mizoguchi, F. Ferri, M. Cocco, and T. Shimamoto (2011). Fault lubrication during earthquakes, *Nature* **471,** 494–499.

Di Toro, G., T. Hirose, S. Nielsen, G. Pennacchioni, and T. Shimamoto (2006). Natural and experimental evidence of melt lubrication of faults during earthquakes, *Science* **311,** 647–649.

Di Toro, G., T. Hirose, S. Nielsen, and T. Shimamoto (2006). Relating high-velocity rock friction experiments to coseismic slip, in *Radiated Energy and the Physics of Faulting*, R. Abercrombie, A. McGarr, G. Di Toro, and H. Kanamori (Editors), Geophysical Monograph Series, Vol. 170, American Geophysical Union, Washington, D.C., 121–134.

Di Toro, G., S. B. Nielsen, E. Spagnuolo, A. R. Niemeijer, S. Smith, and M. E. Violay (2011). Constraints on friction during earthquakes from rock deformation experiments, presented at *2011 Fall Meeting, AGU*, San Francisco, California, 5–9 December, Abstract S53D–01.

Di Toro, G., G. Pennacchioni, and S. Nielsen (2009). Pseudotachylites and earthquake source mechanics, in *Fault-Zone Properties and Earthquake Rupture Dynamics*, E. Fukuyama (Editor), Academic Press, Cambridge, Massachusetts, 87–133.

Di Toro, G., G. Pennacchioni, and G. Teza (2005). Can pseudotachylites be used to infer earthquake source parameters? An example of limitations on the study of exhumed faults, *Tectonophysics* **402,** 3–20.

Dunham, E. M., D. Belander, C. Lin, and J. E. Kozdon (2011). Earthquake ruptures with strongly rate-weakening friction and off-fault plasticity, part 2: Rough faults, *Bull. Seismol. Soc. Am.* **101,** 2308–2322.

Ellsworth, W. L., K. Imanishi, J. Luetgert, J. Kruger, and J. Hamilton (2011). The M_w 5.8 Virginia earthquake of August 23, 2011 and its aftershocks: A shallow high stress drop event, presented at *2011 Fall Meeting, AGU*, San Francisco, California, 5–9 December, Abstract S14B–05.

Escartin, J., G. Hirth, and B. Evans (1997). Nondilatant brittle deformation of serpentinites; implications for Mohr-Coulomb theory and the strength of faults, *J. Geophys. Res.* **102,** 2897–2913.

Fang, Z., and E. Dunham (2013). Additional shear resistance from fault roughness and stress levels on geometrically complex faults, *J. Geophys. Res.* **118,** 1–13, doi: 10.1002/jgrb.50262.

Griffith, W. A., S. Nielsen, G. Di Toro, and S. A. F. Smith (2010). Rough faults, distributed weakening, and off-fault deformation, *J. Geophys. Res.* **115,** no. B08409, doi: 10.1029/2009JB006925.

Hanks, T. C. (1977). Earthquake stress-drops, ambient tectonic stresses, and the stresses that drive plates, *Pure Appl. Geophys.* **115,** 441–458.

Harris, R. A. (2004). Numerical simulations of large earthquakes: Dynamic rupture propagation on heterogeneous faults, *Pure Appl. Geophys.* **161,** 2171–2181, doi: 10.1007/s00024-004-2556-8.

Harris, R. A., M. Barall, R. Archuleta, E. Dunham, B. Aagaard, J. P. Ampuero, H. Bhat, V. Cruz-Atienza, L. Dalguer, P. Dawson, *et al.* (2009). The SCEC/USGS dynamic earthquake rupture code verification exercise, *Seismol. Res. Lett.* **80,** 119–126, doi: 10.1785/gssrl.80.1.119.

Hirose, T., and T. Shimamoto (2003). Fractal dimension of molten surfaces as a possible parameter to infer the slip-weakening distance of faults from natural pseudotachylites, *J. Struct. Geol.* **25,** 1569–1574.

Hirose, T., and T. Shimamoto (2005). Growth of molten zone as a mechanism of slip weakening of simulated faults in gabbro during frictional melting, *J. Geophys. Res.* **110,** no. B05202, doi: 10.1029/2004JB003207.

Ida, Y. (1972). Cohesive force across the tip of a longitudinal shear crack and Griffith's specific surface energy, *J. Geophys. Res.* **77,** 3796–3805.

Ide, S., and G. C. Beroza (2001). Does apparent stress vary with earthquake size? *Geophys. Res. Lett.* **28,** 3349–3352, doi: 10.1029/2001GL013106.

Jeffreys, H. (1942). On the mechanics of faulting, *Geol. Mag.* **79,** 291–295.

Kanamori, H. (1994). The mechanics of earthquakes, *Annu. Rev. Earth Planet. Sci.* **22,** 207–237.

Kanamori, H., and E. E. Brodsky (2004). The physics of earthquakes, *Rept. Progr. Phys.* **67,** 1429–1496, doi: 10.1088/0034-4885/67/8/R03.

Kanamori, H., and T. H. Heaton (2000). Microscopic and macroscopic physics of earthquakes, in *Geocomplexity and the Physics of Earthquakes*,

J. Rundle, D. L. Turcotte, and W. Klein (Editors), Geophys. Monogr. Ser., Vol. 120, AGU, Washington, D.C., 147–155.

Kanamori, H., D. L. Anderson, and T. H. Heaton (1998). Frictional melting during the rupture of the 1994 Bolivian earthquake, *Science* **279,** 839–842.

Kaneko, Y., and P. M. Shearer (2014). Seismic source spectra and estimated stress drop derived from cohesive-zone models of circular subshear rupture, *Geophys. J. Int.* **197,** 1002–1015.

Kim, A., and D. S. Dreger (2008). Rupture process of the 2004 Parkfield earthquake from near-fault seismic waveform and geodetic records, *J. Geophys. Res.* **113,** no. B07308, doi: 10.1029/2007JB005115.

Kirkpatrick, J. D., and C. D. Rowe (2013). Disappearing ink: How pseudotachylites are lost from the rock record, *J. Struct. Geol.* **52,** 183–198.

Kirkpatrick, J. D., Z. K. Shipton, and C. Persano (2009). Pseudotachylytes: Rarely generated, rarely preserved or rarely reported? *Bull. Seismol. Soc. Am.* **99,** 382–388.

Lachenbruch, A. H. (1980). Frictional heating, fluid pressure, and the resistance to fault motion, *J. Geophys. Res.* **85,** 6097–6112.

Lachenbruch, A. H., and J. H. Sass (1980). Heat flow and energetics of the San Andreas fault zone, *J. Geophys. Res.* **85,** 6185–6222.

Lapusta, N., and J. R. Rice (2003). Low-heat and low-stress fault operation in earthquake models of statically strong but dynamically weak faults, *Eos Trans. AGU* **84,** no. 46 (Fall Meet. Suppl.), Abstract S51B–02.

Lavallee, Y., T. Hirose, J. E. Kendrick, K. U. Hess, and D. B. Dingwell (2015). Fault rheology beyond frictional melting, *Proc. Natl. Acad. Sci. Unit States. Am.* **112,** no. 30, 9276–9280, doi: 10.1073/pnas.1413608112.

Lockner, D. A., and P. G. Okubo (1983). Measurements of frictional heating in granite, *J. Geophys. Res.* **88,** 4313–4320.

Ma, K. F., S. R. Song, H. Tanaka, C. Y. Wang, J. H. Hung, Y. B. Tsai, J. Mori, Y. F. Song, E. C. Yeh, H. Sone, *et al.* (2006). Slip zone and energetics of a large earthquake from the Taiwan Chelungpu-fault Drilling Project (TCDP), *Nature* **444,** 473–476.

Madariaga, R. (1976). Dynamics of an expanding circular fault, *Bull. Seismol. Soc. Am.* **66,** 639–666.

Marone, C., C. B. Raleigh, and C. H. Scholz (1990). Frictional behavior and constitutive modeling of simulated fault gouge, *J. Geophys. Res.* **95,** 7007–7025.

Mase, C. W., and L. Smith (1987). Effects of frictional heating on thermal, hydrologic and mechanic response of a fault, *J. Geophys. Res.* **92,** 6249–6272.

McGarr, A. (1994). Some comparisons between mining-induced and laboratory earthquakes, *Pure Appl. Geophys.* **142,** 467–489.

McGarr, A. (1999). On relating apparent stress to the stress causing earthquake fault slip, *J. Geophys. Res.* **104,** 3003–3011.

McKenzie, D., and J. N. Brune (1972). Melting of fault planes during large earthquakes, *Geophys. J. Roy. Astron. Soc.* **29,** 65–78.

Meneghini, F., G. Di Toro, C. D. Rowe, J. C. Moore, A. Tsutsumi, and A. Yamaguchi (2010). Record of mega-earthquakes in subduction thrusts: The black fault rocks of Pasagshak Point (Kodiak Island, Alaska), *Geol. Soc. Am. Bull.* **122,** 1280–1297, doi: 10.1130/B30049.1.

Nielsen, S., G. Di Toro, T. Hirose, and T. Shimamoto (2008). Frictional melt and seismic slip, *J. Geophys. Res.* **113,** no. B01308, doi: 10.1029/2007JB005122.

Nielsen, S., P. Mosca, G. Giberti, G. Di Toro, T. Hirose, and T. Shimamoto (2010). On the transient behavior of frictional melt during seismic slip, *J. Geophys. Res.* **115,** no. B10301, doi: 10.1029/2009JB007020.

Niemeijer, A., G. Di Toro, S. Nielsen, and F. Di Felice (2011). Frictional melting of gabbro under extreme experimental conditions of normal stress, acceleration, and sliding velocity, *J. Geophys. Res.* **116,** no. B07404, doi: 10.1029/2010JB008181.

Noda, H., E. M. Dunham, and J. R. Rice (2009). Earthquake ruptures with thermal weakening and the operation of major faults at low overall stress levels, *J. Geophys. Res.* **114,** no. B07302, doi: 10.1029/2008JB006143.

Orowan, E. (1960). Mechanism of seismic faulting, in *Rock Deformation*, D. Griggs and J. Handin (Editors), Geological Society of America Memoir, Vol. 79, 323–345.

Passelègue, F. X., A. Schubnel, S. Nielsen, H. S. Bhat, and R. Madariaga (2013). From sub-Rayleigh to supershear ruptures during stick-slip experiments on crustal rocks, *Science* **340,** 1208–1211.

Pec, M., H. Stunitz, R. Heilbronner, M. Drury, and C. de Capitani (2012). Origin of psudotachylites in slow creep experiments, *Earth Planet. Sci. Lett.* **355/356,** 299–310.

Pennacchioni, G., G. Di Toro, P. Brack, L. Menegon, and I. M. Villa (2006). Brittle-ductile-brittle deformation during cooling of tonalite (Adamello, Southern Italian Alps), *Tectonophysics* **427,** 171–197.

Pittarello, L., G. Di Toro, A. Bizzarri, G. Pennacchioni, J. Hadizadeh, and M. Cocco (2008). Energy partitioning during seismic slip in pseudotachylyte-bearing faults (Gole Larghe fault, Adamello, Italy), *Earth Planet. Sci. Lett.* **269,** 131–139.

Power, W. L., and T. E. Tullis (1991). Euclidean and fractal models for the description of rock surface roughness, *J. Geophys. Res.* **96,** no. B1, 415–424, doi: 10.1029/90JB02107.

Rice, J. R. (2006). Heating and weakening of faults during earthquake slip, *J. Geophys. Res.* **111,** no. B05311, doi: 10.1029/2005JB004006.

Sagy, A., E. E. Brodsky, and J. G. Axen (2007). Evolution of fault-surface roughness with slip, *Geology* **35,** 283–286.

Sato, T., and T. Hirasawa (1973). Body wave spectra from propagating shear cracks, *J. Phys. Earth* **21,** 415–431.

Savage, J. C., and M. D. Wood (1971). The relation between apparent stress and stress drop, *Bull. Seismol. Soc. Am.* **61,** 1381–1388.

Scholz, C. H. (2002). *The Mechanics of Earthquakes and Faulting*, Second Ed., Cambridge University Press, New York.

Scholz, C. H., C. A. Aviles, and S. G. Wesnousky (1986). Scaling differences between large interplate and intraplate earthquakes, *Bull. Seismol. Soc. Am.* **76,** 65–70.

Sibson, R. H. (1973). Interactions between temperature and pore fluid pressure during earthquake faulting—A mechanism for partial or total stress relief, *Nature* **243,** 66–68.

Sibson, R. H. (1974). Frictional constraints on thrust, wrench and normal faults, *Nature* **249,** 542–544.

Sibson, R. H. (1975). Generation of pseudotachylite by ancient seismic faulting, *Geophys. J. Roy. Astron. Soc.* **43,** 775–794.

Sibson, R. H. (2003). Thickness of the seismic slip zone, *Bull. Seismol. Soc. Am.* **93,** 1169–1178.

Sibson, R. H., and V. G. Toy (2006). The habitat of fault-generated pseudotachylite: Presence vs. absence of friction-melt, in *Radiated Energy and the Physics of Faulting*, R. Abercrombie, A. McGarr, G. Di Toro, and H. Kanamori (Editors), Geophysical Monograph Series, Vol. 170, American Geophysical Union, Washington, D.C., 153–166.

Singh, S. K., and M. Ordaz (1994). Seismic energy release in Mexican subduction zone earthquakes, *Bull. Seismol. Soc. Am.* **84,** 1533–1550.

Sone, H., and T. Shimamoto (2009). Frictional resistance of faults during accelerating and decelerating earthquake slip, *Nat. Geosci.* **2,** 705–708.

Spray, J. G. (1993). Viscosity determinations of some frictionally generated silicate melts: Implications for fault zone rheology at high strain rates, *J. Geophys. Res.* **98,** no. B5, 8053–8068, doi: 10.1029/93jb00020.

Spudich, P. (1992). On the inference of absolute stress levels form seismic radiation, in *Earthquake Source Physics and Earthquake Precursors*, T. Mikumo, K. Aki, M. Ohnaka, L. J. Ruff, and P. K. P. Spudich (Editors), *Tectonophysics* 211, 99–106.

Tajima, R., and F. Tajima (2007). Seismic scaling relations and aftershock activity from the sequences of the 2004 mid Niigata and the 2005 west off Fukuoka earthquakes (M_w 6.6) in Japan, *J. Geophys. Res.* **112,** no. B10302, doi: 10.1029/2007JB004941.

Tinti, E., P. Spudich, and M. Cocco (2005). Earthquake fracture energy inferred from kinematic rupture models on extended faults, *J. Geophys. Res.* **110,** no. B12303, doi: 10.1029/2005JB003644.

Toy, V. G., S. Ritchie, and R. H. Sibson (2011). Diverse habitats of pseudotachylytes in the Alpine fault zone and relationships to current seismicity, *Spec. Publ. Geol. Soc. Lond.* **359,** 115–133, doi: 10.1144/SP359.7.

Tsutsumi, A., and T. Shimamoto (1997). High-velocity frictional properties of gabbro, *Geophys. Res. Lett.* **24,** 699–702.

Ujiie, K., H. Yamaguchi, A. Sakaguchi, and T. Shoichi (2007). Pseudotachylytes in an ancient accretionary complex and implications for melt lubrication during subduction zone earthquakes, *J. Struct. Geol.* **29,** 599–613.

Venkataraman, A., and H. Kanamori (2004). Observational constraints on the fracture energy of subduction zone earthquakes, *J. Geophys. Res.* **109,** no. B5, doi: 10.1029/2003JB002549.

Viegas, G., R. E. Abercrombie, and W.-Y. Kim (2010). The 2002 M5 Au Sable Forks, NY, earthquake sequence: Source scaling relationships and energy budget, *J. Geophys. Res.* **115,** no. B07310, doi: 10.1029/2009JB006799.

Viesca, R. C., and D. I. Garagash (2015). Ubiquitous weakening of faults due to thermal pressurization, *Nat. Geosci.* **8,** no. 11, 875–879, doi: 10.1038/ngeo2554.

Wenk, H.-R., L. R. Johnson, and L. Ratschbacher (2000). Pseudotachylites in the eastern peninsular ranges of California, *Tectonophysics* **321,** 253–277.

Wilson, B., T. Dewers, Z. Reches, and J. Brune (2005). Particle size and energetics of gouge from earthquake rupture zones, *Nature* **434,** 749–752.

Wyss, M. (1970). Stress estimates for South American shallow and deep earthquakes, *J. Geophys. Res.* **75,** 1529–1544, doi: 10.1029/JB075i008p01529.

Zheng, G., and J. R. Rice (1998). Conditions under which velocity-weakening friction allows a self-healing versus a cracklike mode of rupture, *Bull. Seismol. Soc. Am.* **88,** 1466–1483.

Appendix

Estimated Initial Stress

The hypocentral source region of the pseudotachylite at Gole Larghe was at ~10 km depth, in a strike-slip faulting regime in Tonalite (Di Toro and Pennacchioni, 2004; Di Toro *et al.*, 2005). To estimate the ambient stress level, we follow these cited prior studies and assume an Andersonian strike-slip regime (Anderson, 1951) in which the lithostatic stress from overburden σ_L is the mean of the greatest and least principal stresses $\sigma_L = \sigma_m = (\sigma_1 + \sigma_3)/2$. The fault is optimally oriented for failure in the stress field and assumed to limit the stress level in the surrounding rock. These conditions are depicted in the Mohr diagram (Fig. A1), where the fault is assumed to be cohesionless with a friction coefficient $\mu = \tau/\sigma_e$, defining the friction angle $\mu = \tan\phi$, τ is the shear stress, σ_e is the effective normal stress ($\sigma_e = \sigma_n - p$), σ_n is the normal stress, and p is the pore fluid pressure. Here, the ratio of pore pressure to the lithostatic stress is denoted by the ratio $\lambda = p/\sigma_L$ (Sibson, 1974). From the Mohr construction (Fig. A1), effective normal stress is

$$\sigma_e = \sigma_L(1-\lambda)\cos^2\phi. \qquad \text{(A1)}$$

The lithostatic gradient is taken to be 26 MPa/km and $\sigma_L = 260$ MPa. To estimate a representative effective normal stress, we follow Di Toro *et al.* (2005) and average

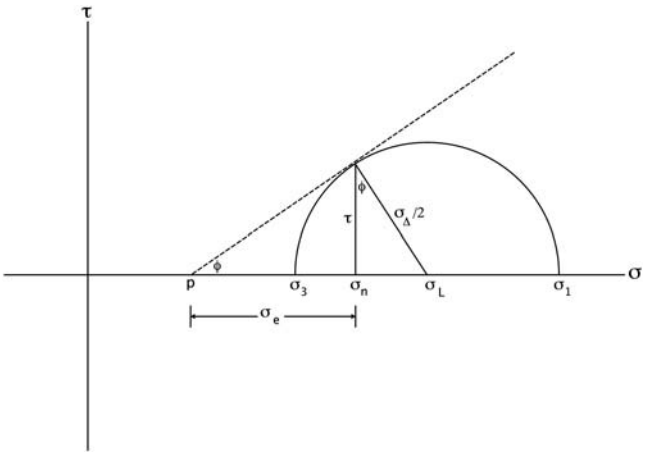

Figure A1. Schematic Mohr diagram of the estimated initial stress state for pseudotachylite at the Gole Larghe fault zone (see the Appendix for the description).

the results from assuming that the pore pressure is hydrostatic with pore pressure gradient 10 MPa/km, with those from assuming dry conditions. That is, using $\lambda = 10/26$ and $\lambda = 0$ in equation (A1), resulting in $\sigma_e = 93$ and 151 MPa, and a representative $\sigma_e = 122$ MPa for $\mu = 0.85$ (Byerlee, 1978) that is appropriate for crystalline rock. These assumptions correspond to a shear resistance at a failure of $\tau = 104$ MPa.

U.S. Geological Survey
Cascades Observatory
1300 Cardinal Court
Building 10, Suite 100
Vancouver, Washington 98683
(N.M.B.)

School of Earth and Environmental Sciences
University of Manchester
Oxford Road
Manchester M139PL, UK
(G.D.)

Department of Earth Sciences
Durham University
Science Labs
Durham DH1 3LE, UK
(S.N.)

Manuscript received 2 December 2015;
Published Online 25 October 2016